Energy Conversion and Management 198 (2019) 111917

Contents lists available at ScienceDirect

Energy Conversion and Management

journal homepage: www.elsevier.com/locate/enconman

Thermally driven refrigerators: Equivalent low-dissipation three-heat-source model and comparison with experimental and simulated results

Juncheng Guo[a,b,*], Hanxin Yang[a], Houcheng Zhang[c], Julian Gonzalez-Ayala[b,d], J.M.M. Roco[b,d], A. Medina[b,d], A. Calvo Hernández[b,d]

[a] College of Physics and Information Engineering, Fuzhou University, Fuzhou 350116, PR China
[b] Department of Applied Physics, University of Salamanca, 37008 Salamanca, Spain
[c] Department of Microelectronic Science and Engineering, Ningbo University, Ningbo 315211, China
[d] Instituto Universitario de Física Fundamental y Matemáticas (IUFFyM), University of Salamanca, 37008 Salamanca, Spain

ARTICLE INFO

Keywords:
Thermally driven refrigerator
Low-dissipation assumption
Three-heat-source refrigerator model
Bound of performance coefficient
Comparison with experimental data

ABSTRACT

In order to investigate the performance of a class of thermally driven refrigerators, usually driven by low-grade thermal energy, a generic thermodynamic model of three-heat-source refrigerator without involving any specific heat-transfer law is put forward by adopting low-dissipation assumptions. Based on the proposed model, the analytical expressions for the coefficient of performance (COP) and cooling power of the system are derived in terms of well-defined dissipation parameters and contact time durations between the system and heat reservoirs. One essential parameter accounting for the size ratio of the two coupled subsystems inside the overall system is introduced in light of the practical meaning of the reversible entropy change. With the help of the aforementioned parameter, the optimal relation between the COP and cooling power is obtained. The optimal operation region and optimal construction of the overall system are further determined for the first time. In addition, the influences of the dissipation and temporal symmetries are discussed in detail, according to which the upper and lower bounds of the COP at maximum cooling power are firstly obtained under two extreme situations. Experimental and simulated data from previous reported works are collected to illustrate the validity and practical significance of the proposed model and associated results. A limit case is presented to highlight the generality of the model.

1. Introduction

Nowadays, the efficient utilizations of low-grade (LG) thermal energy from several sources, such as biomass energy, geothermal energy, solar energy, and industrial waste heats, are deemed as a vital solution in the face of the challenges of the constantly increasing energy demand, the rapid depletion of fossil fuels, and the related environment impacts [1]. Various LG heat harvesting technologies have been put forward continually [2–5]. Among all these feasible proposals, a class of thermally driven refrigerators, mainly including absorption refrigerator [6–8], adsorption refrigerator [9–11], and ejector refrigerator [12–14], are particularly attractive to researchers due to the fact that around 15% of the electricity generated worldwide is consumed by air-conditioning processes [15]. As the promising alternatives of traditional vapor compression refrigerator, thermally driven refrigerators possess the merits of fewer moving parts, low noise, high reliability, low operation cost, long lifetime, adaptability to a wide range of heat source temperatures, and the possibility of using environmentally-friendly refrigerants [16–18]. Nevertheless, although thermally driven refrigerators seem to provide the aforementioned advantages, they still suffer the bottleneck of poor overall performance which greatly limits their applications and commercialization [17–19]. Therefore, further investigations and improvements of the performance of thermally driven refrigerators are highly desirable for both researchers and engineers.

In order to make use of LG thermal energy, thermally driven refrigerators should work among more than two heat reservoirs. Besides, generator, absorber, adsorber, desorber, or ejector are adopted by different thermally driven refrigerators, respectively, to fulfill the function of compressor. In spite of the different components, working fluids, circulation modes, etc., various thermally driven refrigerators have, in essence, identical operation principle from the perspective of thermodynamics. Specifically, based on classical thermodynamics, a reversible three-heat-source (THS) refrigerator cycle, which is equivalent to a

* Corresponding author.
E-mail address: junchengguo@qq.com (J. Guo).

https://doi.org/10.1016/j.enconman.2019.111917
Received 11 May 2019; Received in revised form 1 August 2019; Accepted 4 August 2019
0196-8904/ © 2019 Elsevier Ltd. All rights reserved.

Nomenclature

Latin letters

B	size ratio of two subsystems
R	cooling power (W)
$\tilde{R}$	dimensionless cooling power
S	entropy (JK^{-1})
T	temperature (K)
$\tilde{T}$	dimensionless temperature
t	time (s)
$\tilde{t}$	dimensionless time
W	work (J)

Greek letters

β	dissipation symmetry between two subsystems
γ	temporal symmetry between two subsystems
ε	coefficient of performance of Carnot refrigerator
η	efficiency of Carnot heat engine
σ	dissipation parameter (s)
$\tilde{\sigma}$	dimensionless dissipation parameter
τ	cycle time (s)
$\tilde{\tau}$	dimensionless cycle time
ψ	coefficient of performance of the three-heat-source refrigerator

Subscript

B	given size ratio state
C	low temperature side/source
H	high temperature side/source
he	heat engine
max	maximum
min	minimum
O	intermediate temperature side/source
Rm	maximum cooling power state
r	reversible condition
re	refrigerator

Abbreviations

COP	coefficient of performance
LD	low-dissipation
LG	low-grade
THS	three-heat-source

reversible Carnot refrigerator driven by a reversible Carnot heat engine, may be used to describe a class of thermally driven refrigerators when all the irreversibilities are ignored [20,21]. As a result, the coefficient of performance (COP) of the refrigerator can be expressed as [20]

$$\psi_r = \frac{T_C}{T_H}\frac{T_H - T_O}{T_O - T_C} \tag{1}$$

where T_H, T_O, and T_C are respectively the temperatures of LG heat source, environment, and cooled space. The value of ψ_r provides a ceiling limit of the COP that the THS refrigerator operated between three heat reservoirs with different temperatures can achieve. However, ψ_r can be only reached at the quasistatic limit where the transformation of the system should proceed infinitely slow and the corresponding cooling power is equal to zero. Hence, huge deviations between ψ_r and experimental values always exist, which implies that more practical and realistic models for THS refrigerators are necessary.

In this regard, endoreversible THS refrigerator thermodynamic cycle models have been established to investigate the performance characteristics of the practical thermally driven refrigerators with finite cooling power. With the help of it, the influences of irreversibilities associated to the heat-transfer processes between working substance and heat reservoirs, internal dissipations in the working substance, and external heat leakage losses have been discussed [21–26]. Besides, various figures of merit such as thermo-ecological, thermoeconomic, and ecological functions have been introduced to evaluate the performance of the system [16,27–29]. In addition, many more realistic and meaningful results have been obtained with this model by adopting different heat-transfer laws and heat-transfer processes with finite heat capacity [30–34] and constructing different hybrid systems [35–37].

However, in spite of the significant obtained results, the inherent drawback of endoreversible thermodynamic model, namely, the dependence of the performance characteristic on specific heat-transfer law, motivates researchers to keep exploring the way of establishing a more universal thermodynamic model without invoking any specific heat-transfer law. After detailed analyses of several different thermodynamic systems, an innovative thermodynamic cycle of Carnot heat engine has been proposed by adopting low-dissipation (LD) assumptions [38]. In this model, specific laws of heat-transfer have been replaced by non-negative parameters containing information about irreversibilities, thus allowing to analyze the dissipation symmetry/asymmetry in the model. Based on the proposed LD model, the expression of the efficiency at maximum power output has been derived. Some significant results deduced from endoreversible cycle model can be directly recovered under different dissipation symmetry situations [38]. More importantly, the upper and lower bounds for the efficiency at maximum power output can be obtained at two extreme asymmetry dissipation situations, respectively, which fits quite well with the efficiencies of various practical heat engines [38].

Due to its generality and the consistent results with reality, LD models have become a hot research topic in recent years. They have been further developed and applied to investigate the performance characteristics of several thermodynamic devices by many researchers [39–44]. Besides, different objective functions [44–46] and constraint conditions [46–48] have been introduced to assess the performance characteristics of the models. Moreover, the relations between minimally nonlinear irreversible models [49,50], endoreversible models [51,52], and LD models have also gained the interest of many authors.

According to all the comments above, an interesting question arises: is it possible to establish a more universal model of THS refrigerator by adopting LD assumptions to obtain more practical results? According to the literature review, this important task has not been accomplished yet. Therefore, the main objective of present paper is to further develop the LD thermodynamic model and bridge this knowledge gap, which is of theoretical and practical significance.

The organization of the present paper is as follows. In Section 2, several typical examples of thermally driven refrigerators followed by a universally equivalent LD THS model are presented. In Section 3, analytical expressions for COP and cooling power are driven. Besides, a crucial parameter in regard to the entropy generations of the subsystems is introduced and stressed due to its pivotal role both in theory and practice. Then, the optimal relation between COP and cooling power is discussed in Section 4. In Section 5, numerical calculation is used to investigate the optimal performance characteristics of the system, according to which the optimal operation strategies can be determined. Besides, the influences of the dissipation symmetry, temporal symmetry, and several important parameters on the performance of the system are evaluated. In Section 6, the optimal parametric design, specifically, the optimal construction of the THS refrigerator is analyzed by which the upper and lower bounds of the COP at maximum cooling power are further obtained for the first time. In Section 7,

experimental and simulated data from previous literatures are collected to validate the proposed model and the obtained upper and lower bounds. In addition, a limit case which emphasizes the generalization of the THS refrigerator model is presented. To conclude, the most significant results obtained in the present paper are summarized and the potential applications of the LD THS model are prospected.

2. Typical thermally driven refrigerators and their equivalent low-dissipation three-heat-source combined cycle model

The schematic diagrams of three typical thermally driven refrigerators, i.e., absorption refrigeration, adsorption refrigeration, and ejector refrigeration, are shown in Fig. 1(a)–(c), respectively. It can be seen from Fig. 1 that the compressor adopted by traditional refrigerators has been replaced by various components, which have been marked by red dashed line. To be more specific, generator and absorber are adopted for absorption refrigeration, desorber and adsorber are used to construct adsorption refrigerator, and generator and ejector are applied to build ejector refrigerator. More importantly, instead of consuming electricity, thermal energy, usually LG thermal energy, can be used to drive these refrigerator systems. In Fig. 1, Q_H, Q_{OH}, Q_{OC}, and Q_C indicate the heat absorbed from high-temperature reservoir, the heats released into environment, and the heat absorbed from cooled space during one cycle, respectively.

Despite the different components, circulation modes, and working substances involved in these different types of thermally driven refrigerators (see Fig. 1), all of them have the similarity of fundamental working principle from the perspective of thermodynamics. Therefore, instead of discussing the details of the specific systems, a generic and equivalent thermodynamic model, which is heat-transfer-independent and may be used to describe a class of irreversible thermally driven refrigerators, will be presented by using LD assumptions [38].

The key point in our proposition of the generic thermodynamic model for THS refrigerator is the introductions of low-dissipation assumptions and the size ratio of two subsystems (the Carnot refrigerator and Carnot heat engine) inside the overall system. The former overcomes the dependence of the performance characteristics on specific heat-transfer law and allows to analyze the temporal and dissipation symmetry, which leads to the upper and lower bounds of the COP at maximum cooling power of the THS system. The latter plays an important role in connecting two subsystems insides the overall system thus allowing the analysis of the optimal relation between COP and cooling power for the overall system.

Based on LD assumptions [38], an equivalent LD THS refrigerator consisting of a LD Carnot heat engine and a LD Carnot refrigerator with well-defined contact time durations and related dissipation parameters is established, as shown in Fig. 2. In this model, Q_H, Q_{OH}, Q_{OC}, and Q_C are the heats exchanged between three heat reservoirs and the THS refrigerator per cycle; t_H, t_{OH}, t_{OC}, and t_C are the corresponding time durations of four heat-transfer processes within the Carnot heat engine and Carnot refrigerator during one cycle; σ_H, σ_{OH}, σ_{OC}, and σ_C are the associated non-negative dissipation parameters involving specifically irreversible information. Besides, the dissipations inside the model are expected to behave as σ_H/t_H, σ_{OH}/t_{OH}, σ_{OC}/t_{OC}, and σ_C/t_C by neglecting the relaxation time of the working substance and the more complicated time-dependence dissipation terms.

Besides, it should be pointed out that the values of dissipation parameters depend on the characteristics of specific systems and are difficult to be determined for practical devices. The significance of the establishment of the LD THS thermodynamic model is its generality and the relevant symmetry analyses and optimizations based on it.

3. Coefficient of performance and cooling power

According to the proposed model of THS refrigerator above, Q_H, Q_{OH}, Q_{OC}, and Q_C can be expressed as [38–40]

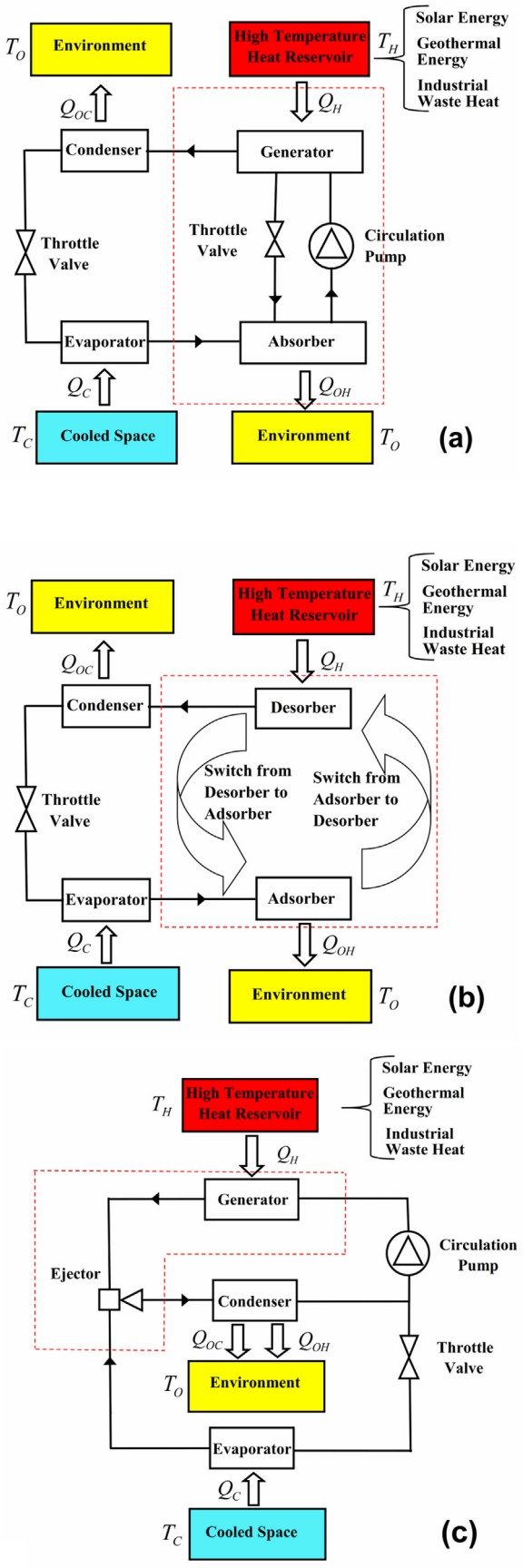

Fig. 1. Schematic diagrams of three typical thermally driven refrigerators: (a) absorption refrigeration, (b) adsorption refrigeration, and (c) ejector refrigeration.

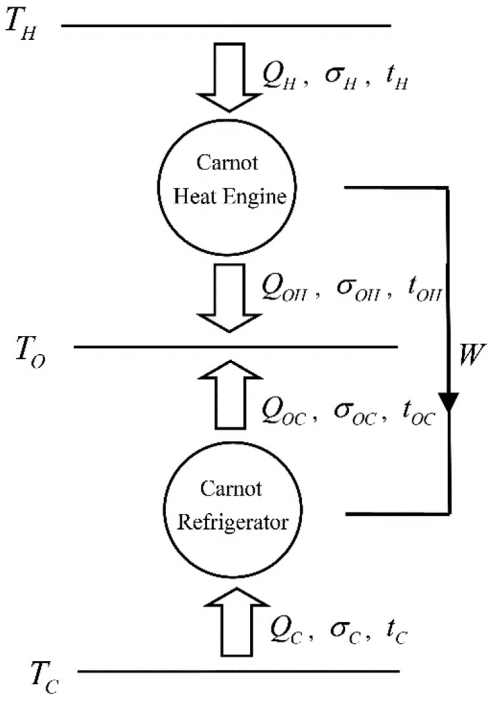

Fig. 2. Equivalent low-dissipation three-heat-source refrigerator model.

$$Q_H = Q_{Hr}\left(1 - \frac{\sigma_H}{t_H}\right) = T_H \Delta S_{he}\left(1 - \frac{\sigma_H}{t_H}\right) \tag{2}$$

$$Q_{OH} = Q_{OHr}\left(1 + \frac{\sigma_{OH}}{t_{OH}}\right) = T_O \Delta S_{he}\left(1 + \frac{\sigma_{OH}}{t_{OH}}\right) \tag{3}$$

$$Q_{OC} = Q_{OCr}\left(1 + \frac{\sigma_{OC}}{t_{OC}}\right) = T_O \Delta S_{re}\left(1 + \frac{\sigma_{OC}}{t_{OC}}\right) \tag{4}$$

and

$$Q_C = Q_{Cr}\left(1 - \frac{\sigma_C}{t_C}\right) = T_C \Delta S_{re}\left(1 - \frac{\sigma_C}{t_C}\right) \tag{5}$$

respectively, where $Q_{Hr} = T_H \Delta S_{he}$, $Q_{OHr} = T_O \Delta S_{he}$, $Q_{OCr} = T_O \Delta S_{re}$, and $Q_{Cr} = T_C \Delta S_{re}$ are, respectively, the heats absorbed from high-temperature reservoir and released into intermediate-temperature reservoir by Carnot heat engine and the heats released into intermediate-temperature reservoir and absorbed from low-temperature reservoir by Carnot refrigerator under reversible condition. ΔS_{he} and ΔS_{re} indicate the reversible entropy changes of the Carnot heat engine and Carnot refrigerator, respectively. It can be seen from Eqs. (2)–(5) that a reversible THS refrigerator will be recovered from the LD model when $t_H \to \infty$, $t_{OH} \to \infty$, $t_{OC} \to \infty$, and $t_C \to \infty$, which is consistent with the key assumption of the LD model [38].

It is worthy to notice that in previous researches the reversible entropy changes in the LD thermodynamic models operated only between two reservoirs were usually adopted as a factor which made the performance parameters such as power output, cooling power, heating load, etc., dimensionless. Therefore, their values are somewhat irrespective of the performance characteristics and seems to be trivial [40,43,47,48,52]. Nevertheless, this claim is invalid in terms of the LD models composed of two LD subsystems. Specifically, for the LD THS refrigerator, it is of great significance to consider the relation between ΔS_{he} and ΔS_{re} by emphasizing their physical meanings in practice, i.e., the measure of the sizes of the corresponding heat devices [46,48], and the great influence of the matching between the two subsystems on the performance characteristics of the global system. Using Eqs. (2)–(5) and the law of energy conservation, one can drive the relation between ΔS_{he} and ΔS_{re} as

$$\frac{\Delta S_{re}}{\Delta S_{he}} = \frac{T_H\left(1 - \frac{\sigma_H}{t_H}\right) - T_O\left(1 + \frac{\sigma_{OH}}{t_{OH}}\right)}{T_O\left(1 + \frac{\sigma_{OC}}{t_{OC}}\right) - T_C\left(1 - \frac{\sigma_C}{t_C}\right)} = B \tag{6}$$

where B denotes the size ratio of the Carnot refrigerator to Carnot heat engine and is required to keep constant in the light of the reality that practical THS refrigerators have fixed size ratio. Besides, the value range of B can be determined from Eq. (6), i.e.,

$$0 < B < B_r \tag{7}$$

where $B_r = (T_H - T_O)/(T_O - T_C)$ is the value of B under reversible condition. B plays an important role in connecting LD Carnot heat engine and Carnot refrigerator and its effects on the performance of the overall system will be discussed at length in the subsequent sections.

If the time durations of the four adiabatic processes of the Carnot heat engine and Carnot refrigerator are further assumed to be negligible, the whole cycle time of the global system can be approximately expressed as $\tau = t_H + t_{OH} + t_{OC} + t_C$. Consequently, the cooling power and COP of the system can be deduced by using Eqs. (2)–(6) as

$$R = \frac{Q_C}{\tau} = \frac{T_C \Delta S_{re}\left(1 - \frac{\sigma_C}{t_C}\right)}{t_H + t_{OH} + t_{OC} + t_C} \tag{8}$$

and

$$\psi = \frac{Q_C}{Q_H} = \varepsilon\eta = B\frac{T_C\left(1 - \frac{\sigma_C}{t_C}\right)}{T_H\left(1 - \frac{\sigma_H}{t_H}\right)} \tag{9}$$

respectively, where $\eta = W/Q_H$ is the efficiency of the Carnot heat engine, $\varepsilon = Q_C/W$ is the COP of the Carnot refrigerator, $W = Q_H - Q_{OH} = Q_{OC} - Q_C$ is the work output of the Carnot heat engine per cycle and also the work input of the Carnot refrigerator during one cycle (see Fig. 2).

4. Optimal relation between the coefficient of performance and the cooling power

It can be found out from Eq. (9) that the COP of the LD THS refrigerator attains its optimum at the conditions which make both η and ε optimum. Therefore, in order to obtain the optimal value of ψ, the optimization of η and ε should be discussed first. Based on the established LD model above, the efficiency of the LD Carnot heat engine can be expressed as

$$\eta = 1 - \frac{Q_{OH}}{Q_H} = 1 - \frac{\left(1 + \frac{1 - \tilde{\sigma}_H}{\tilde{\tau}_{he} - \tilde{t}_H}\right)}{\tilde{T}_H\left(1 - \frac{\tilde{\sigma}_H}{\tilde{t}_H}\right)} \tag{10}$$

where $\tilde{T}_H = T_H/T_O$, $\tilde{\sigma}_H = \sigma_H/(\sigma_H + \sigma_{OH})$, $\tilde{\tau}_{he} = (t_H + t_{OH})/(\sigma_H + \sigma_{OH})$, $\tilde{t}_H = t_H/(\sigma_H + \sigma_{OH})$. By using Eq. (10) and solving the extremal condition $(\partial\eta/\partial\tilde{t}_H)_{\tilde{\tau}_{he}} = 0$, the optimal relation between $\tilde{t}_H$ and $\tilde{\tau}_{he}$, which makes η optimal, can be obtained as

$$\tilde{t}_H = \begin{cases} \frac{\tilde{\sigma}_H\tilde{\tau}_{he} - \sqrt{\tilde{\sigma}_H\tilde{\tau}_{he}[\tilde{\tau}_{he} - (2\tilde{\sigma}_H - 1)](1 - \tilde{\sigma}_H)}}{2\tilde{\sigma}_H - 1} & \cdot \ \tilde{\sigma}_H \neq 0.5 \\ \frac{1 + 2\tilde{\tau}_{he}}{4} & \cdot \ \tilde{\sigma}_H = 0.5 \end{cases} \tag{11}$$

Likewise, the COP of the LD Carnot refrigerator can be expressed as

$$\varepsilon = \frac{Q_C}{Q_{OC} - Q_C} = \frac{\tilde{T}_C\left(1 - \frac{\tilde{\sigma}_C}{\tilde{t}_C}\right)}{\left(1 + \frac{1 - \tilde{\sigma}_C}{\tilde{\tau}_{re} - \tilde{t}_C}\right) - \tilde{T}_C\left(1 - \frac{\tilde{\sigma}_C}{\tilde{t}_C}\right)} \tag{12}$$

according to the proposed LD model, where $\tilde{T}_C = T_C/T_O$, $\tilde{\sigma}_C = \sigma_C/(\sigma_C + \sigma_{OC})$, $\tilde{\tau}_{re} = (t_C + t_{OC})/(\sigma_C + \sigma_{OC})$, $\tilde{t}_C = t_C/(\sigma_C + \sigma_{OC})$. Using Eq. (12) and the extremal condition $(\partial\varepsilon/\partial\tilde{t}_C)_{\tilde{\tau}_{re}} = 0$, one can prove that when the relation

$$\tilde{t}_C = \begin{cases} \dfrac{\tilde{\sigma}_C\tilde{\tau}_{re} - \sqrt{\tilde{\sigma}_C\tilde{\tau}_{re}[\tilde{\tau}_{re} - (2\tilde{\sigma}_C - 1)](1-\tilde{\sigma}_C)}}{2\tilde{\sigma}_C - 1} & \tilde{\sigma}_C \neq 0.5 \\ \dfrac{1+2\tilde{\tau}_{re}}{4} & \tilde{\sigma}_C = 0.5 \end{cases} \tag{13}$$

is satisfied, the value of ε is optimal.

Besides, based on Eq. (8) a dimensionless cooling power of the overall system can be introduced for the convenience of discussion, namely,

$$\tilde{R} = \frac{R(\sigma_H + \sigma_{OH})}{T_O \Delta S_{he}} = \frac{\tilde{T}_C B\left(1 - \frac{\tilde{\sigma}_C}{\tilde{t}_C}\right)}{\tilde{\tau}_{he} + \tilde{\tau}_{re}\frac{1-\beta}{\beta}} \tag{14}$$

where $\beta = (\sigma_H + \sigma_{OH})/(\sigma_H + \sigma_{OH} + \sigma_C + \sigma_{OC})$ accounts for the dissipation symmetry between the Carnot heat engine and the Carnot refrigerator.

According to the above analyses, the optimal relations between the COP and cooling power can be obtained by using Eqs. (6), (9), (11), (13), and (14). Unfortunately, the analytical results are unachievable, so they will be investigated by means of numerical calculation in the next section. In particular, the dependence of the performance characteristics on the following parameters will be discussed in detail: dissipation parameters $\tilde{\sigma}_H$ and $\tilde{\sigma}_C$; time durations $\tilde{\tau}_{he}$ and $\tilde{\tau}_{re}$; reservoir temperatures $\tilde{T}_H$ and $\tilde{T}_C$; size ratio B; dissipation symmetry parameter β.

5. Optimal operation strategies

5.1. Optimal relation between coefficient of performance and cooling power

Using Eqs. (6), (9), (11), (13), (14), and numerical calculation, one can obtain the behaviors of optimized COP with the corresponding cooling power for different values of B, as shown in Fig. 3, where $\tilde{T}_H = 2$ and $\tilde{T}_C = 0.8$ are selected in order to cover the main operating temperature region of thermally driven refrigerators. It can be seen from Fig. 3 that $\tilde{R}$ is not a monotonic function of ψ for a given value of B. More specifically, the curves of $\tilde{R} - \psi$ for different given values of B are parabolic-like. As a result, there exist a maximum COP $\psi_{\max,B}$ and a minimum COP $\psi_{\min,B}$ at which the cooling power is zero for a given value of B. More importantly, an optimal COP $\psi_{Rm,B}$ exists for a given value of B at which the cooling power reach its maximum $\tilde{R}_{\max,B}$. Note that in Fig. 3 $\psi_{\min,B}$, $\psi_{\max,B}$, and $\psi_{Rm,B}$ increase with the increase of B.

Fig. 3 also shows that for a given value of B, when $\tilde{R} < \tilde{R}_{\max,B}$ there exist two corresponding ψ for a given $\tilde{R}$ lying in two different regions separated by $\psi_{Rm,B}$. It is easy to realize that comparing any point in the region $\psi_{min,B} < \psi < \psi_{Rm,B}$, there always exists a corresponding point in the region $\psi_{max,B} > \psi > \psi_{Rm,B}$ with the same value of $\tilde{R}$ but a larger value of ψ. As a consequence, the optimal operating region of the LD THS refrigerator should be located in the region $\psi_{max,B} > \psi > \psi_{Rm,B}$.

To the best our knowledge, these optimal performance characteristics of THS refrigerator deduced specifically from the LD model have never been reported before. It is the first important result of this paper.

5.2. Dependence on the temporal symmetry

In order to investigate the influence of temporal symmetry, an important control parameter, $\gamma = \tilde{\tau}_{he}/(\tilde{\tau}_{he} + \tilde{\tau}_{re})$, is introduced. It denotes the ratio of the Carnot heat engine cycle time to the overall Carnot cycle time and can be regarded as the measure of the temporal symmetry of the global system. The variations of optimized COP and the corresponding cooling power with γ are presented in Fig. 4 by using Eqs. (6), (9), (11), (13), (14), and numerical calculation. It can be seen from Fig. 4 that optimized COPs decrease monotonically with the increase of γ, whereas the relations between $\tilde{R}$ and γ are not monotonic. An optimal $\gamma_{Rm,B}$ exists leading to maximum cooling power $\tilde{R}_{\max,B}$. According to the analyses in the last subsection, the optimal operating region of γ can be determined as $0 < \gamma < \gamma_{Rm,B}$. In addition, Fig. 4 shows that $\gamma_{Rm,B}$ decreases with the increase of B. Moreover, when $\gamma = 0$ or $\gamma = 1$, i.e., the whole cycle time is distributed to the Carnot refrigerator or the Carnot heat engine, the cooling power of the overall system is zero. In other words, under these conditions the LD THS refrigerator is dysfunctional, which is an expected result.

Besides, a three-dimensional figure is shown in Fig. 5 to reveal the dependence of $\gamma_{Rm,B}$ on the values of $\tilde{\sigma}_H$ and $\tilde{\sigma}_C$ by the same procedure. Fig. 5 shows that the variations of $\gamma_{Rm,B}$ with $\tilde{\sigma}_H$ and $\tilde{\sigma}_C$ are not monotonic but approximately saddle-shaped. Specifically, optimal values of $\tilde{\sigma}_H$ and $\tilde{\sigma}_C$ exist, which make $\gamma_{Rm,B}$ reach its minimum and maximum, respectively, for given values of other parameters.

5.3. Dependence on dissipation symmetry

Similarly, using Eqs. (6), (9), (11), (13), (14), and numerical calculation, one can plot the optimal curves of $\tilde{R} - \psi$ for different values of β, $\tilde{\sigma}_H$, and $\tilde{\sigma}_C$, as shown in Figs. 6 and 7. It can be found out from Fig. 6 that $\tilde{R}$ and $\tilde{R}_{\max,B}$ increase with the increase of β for given values of other parameters, which agrees with Eq. (14). Besides, $\psi_{Rm,B}$ increases with the increase of β which is an expected result, because Eqs. (2)–(5) and the definition of β imply that the greater the value of β is, the less heat is absorbed from high-temperature or the more heat is absorbed from cooled space for given values other parameters. Moreover, Figs. 6 and 7 indicate that the value of $\psi_{\max,B}$ is determined by $\tilde{\sigma}_C$ and $\psi_{\min,B}$ is dependent of $\tilde{\sigma}_H$, whereas they are β-independent.

In order to obtain additional insights in the behaviors of $\psi_{Rm,B}$ and $\tilde{R}_{\max,B}$ varying with $\tilde{\sigma}_H$ and $\tilde{\sigma}_C$, which cannot be easily realized from Fig. 7, two three-dimensional graphs are generated by the same way, as shown in Figs. 8 and 9, respectively. It is shown by Fig. 8 that the variations of $\tilde{R}_{\max,B}$ with $\tilde{\sigma}_H$ and $\tilde{\sigma}_C$ are not monotonic and there exist optimal values of $\tilde{\sigma}_H$ and $\tilde{\sigma}_C$ which lead to the minimum value of $\tilde{R}_{\max,B}$. Meanwhile, Fig. 9 shows that for a given value of $\tilde{\sigma}_C$, $\psi_{Rm,B}$ is a monotonically growing function of $\tilde{\sigma}_H$. On the contrary, $\psi_{Rm,B}$ is a monotonically decreasing function of $\tilde{\sigma}_C$ for a given value of $\tilde{\sigma}_H$. This result is in accordance with our expectations. To be specific, for given values of other parameters, more heat can be absorbed from cooled space with the decrease of $\tilde{\sigma}_C$ and less heat is required to be provided by the high-temperature reservoir with the increase of $\tilde{\sigma}_H$, which can be realized from Eqs. (2), (5), and (9). Besides, it can be seen from Fig. 9 that for a THS refrigerator with a given value of size ratio, the COP at maximum cooling power attains its maximum and minimum at the conditions $\tilde{\sigma}_H = 1$, $\tilde{\sigma}_C = 0$ and $\tilde{\sigma}_H = 0$, $\tilde{\sigma}_C = 1$, respectively. According to the analyses about Figs. 6 and 9, the upper and lower bounds of the COP at maximum cooling power for a THS refrigerator with a given value of size ratio can be further generated. Beyond these particular bounds, more universal and meaningful upper and lower bounds of the

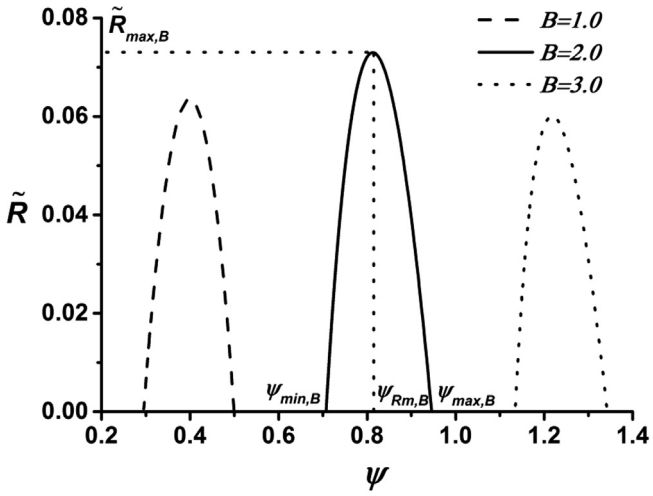

Fig. 3. The behaviors of optimized ψ with the corresponding $\tilde{R}$ for different values of B. $\tilde{\sigma}_H = \tilde{\sigma}_C = 0.3$, $\beta = 0.5$, $\tilde{T}_H = 2$ and $\tilde{T}_C = 0.8$ ($B_r = 5.0$).

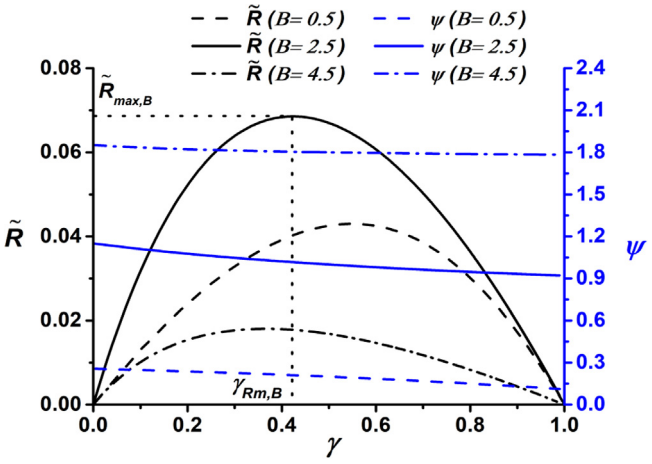

Fig. 4. The variations of optimized ψ and the corresponding $\tilde{R}$ with γ for different values of B. $\tilde{\sigma}_H = \tilde{\sigma}_C = 0.3$, $\beta = 0.5$, $\tilde{T}_H = 2$, and $\tilde{T}_C = 0.8$ ($B_r = 5.0$).

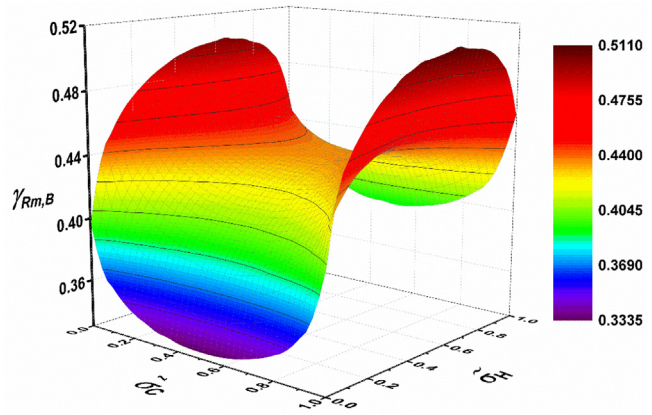

Fig. 5. Three-dimensional graph of $\gamma_{Rm,B}$ varying with $\tilde{\sigma}_H$ and $\tilde{\sigma}_C$. $B = 2.5$, $\beta = 0.5$, $\tilde{T}_H = 2$ and $\tilde{T}_C = 0.8$ ($B_r = 5.0$).

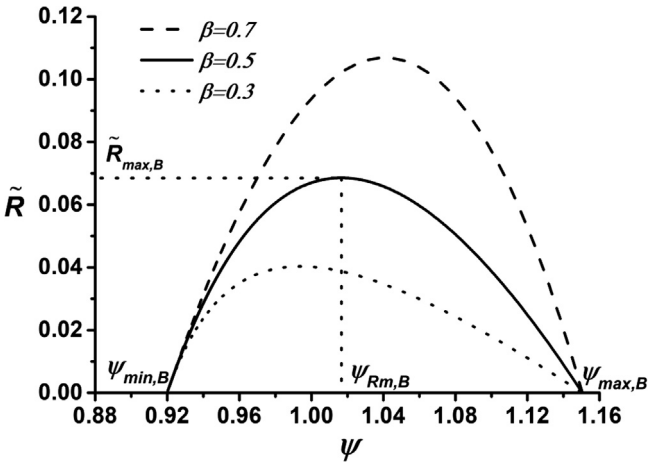

Fig. 6. The variation of optimized ψ with the corresponding $\tilde{R}$ for different values of β. $\tilde{\sigma}_H = \tilde{\sigma}_C = 0.3$, $B = 2.5$, $\tilde{T}_H = 2$ and $\tilde{T}_C = 0.8$ ($B_r = 5.0$).

COP at maximum cooling power can be obtained in terms of all B values. This point will be presented and discussed in the next section.

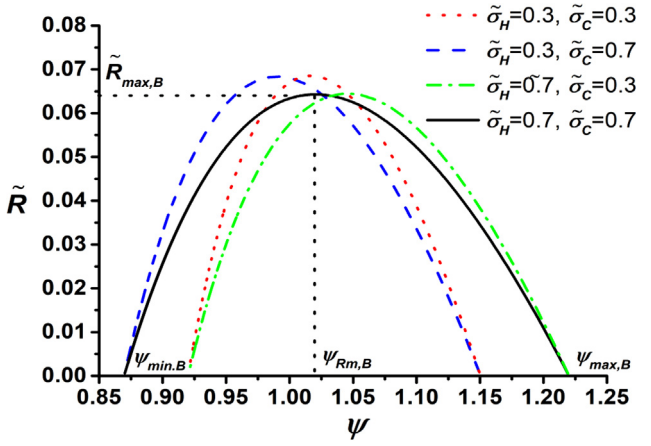

Fig. 7. The variation of optimized ψ with the corresponding $\tilde{R}$ for different values of $\tilde{\sigma}_H$ and $\tilde{\sigma}_C$. $B = 2.5$, $\beta = 0.5$, $\tilde{T}_H = 2$ and $\tilde{T}_C = 0.8$ ($B_r = 5.0$).

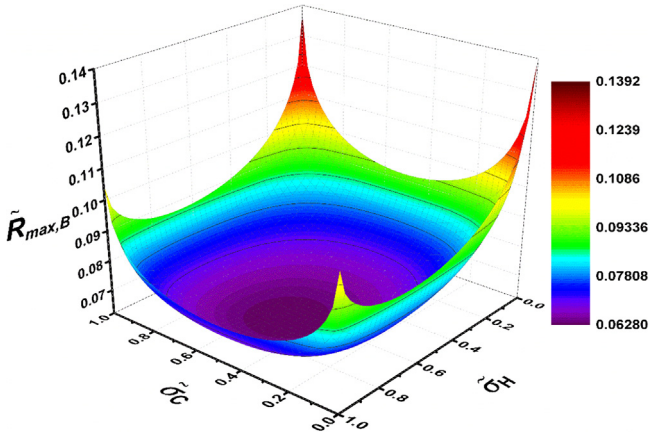

Fig. 8. Three-dimensional graph of $\tilde{R}_{max,B}$ varying with $\tilde{\sigma}_H$ and $\tilde{\sigma}_C$. $B = 2.5$, $\beta = 0.5$, $\tilde{T}_H = 2$ and $\tilde{T}_C = 0.8$ ($B_r = 5.0$).

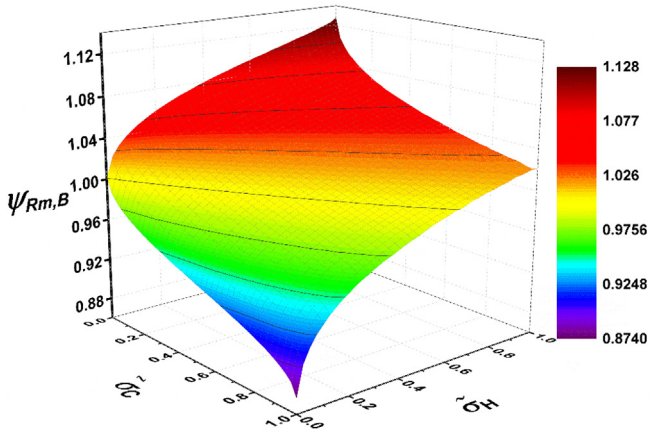

Fig. 9. Three-dimensional graph of $\psi_{Rm,B}$ varying with $\tilde{\sigma}_H$ and $\tilde{\sigma}_C$. $B = 2.5$, $\beta = 0.5$, $\tilde{T}_H = 2$ and $\tilde{T}_C = 0.8$ ($B_r = 5.0$).

6. Bounds of coefficient of performance at maximum cooling power

6.1. Optimal construction (size ratio) of the low-dissipation three-heat-source refrigerator

It can be seen from Figs. 3 and 4 that the value of $\tilde{R}_{max,B}$ is not a monotonic function of B. Using the data in Fig. 3, Eqs. (6), (9), (11),

(13), (14), and numerical calculation, one can plot the variations of $\tilde{R}_{\max,B}$ with B and $\psi_{Rm,B}$ for different values of β and different values of $\tilde{\sigma}_H$ and $\tilde{\sigma}_C$, as shown in Figs. 10 and 11, respectively. These figures indicate that for given temperatures of reservoirs, there is an optimal value of size ratio B_{Rm} that makes $\tilde{R}_{\max,B}$ attain its maximum value $\tilde{R}_{\max}$ at which the corresponding COP is ψ_{Rm}. On the basis of the similar analyses about the optimal operation region in Fig. 3, for given values of $\tilde{T}_H$ and $\tilde{T}_C$, the construction (size ratio) of the LD THS refrigerator should be located in the region $B_r > B > B_{Rm}$ which makes the system work in the region with negative slope, i.e., $\psi_r > \psi > \psi_{Rm}$.

Besides, Fig. 10 shows that the value of ψ_{Rm} increases with the increase of β. Meanwhile, it is shown by Fig. 11 that ψ_{Rm} attains its maximum at the condition $\tilde{\sigma}_H \to 1$ and $\tilde{\sigma}_C \to 1$ and attains its minimum at the condition $\tilde{\sigma}_H \to 0$ and $\tilde{\sigma}_C \to 0$.

6.2. Bounds of the coefficient of performance at maximum cooling power

The combination of the discussions about Figs. 10 and 11 above leads to the important conclusion that ψ_{Rm} attains its maximum at the condition $\tilde{\sigma}_H \to 1$, $\tilde{\sigma}_C \to 1$, and $\beta \to 1$, while it attains its minimum at the condition $\tilde{\sigma}_H \to 0$, $\tilde{\sigma}_C \to 0$, and $\beta \to 0$. Consequently, the upper and lower bounds of $\psi_{Rm} - \tilde{T}_H$ and $\psi_{Rm} - \tilde{T}_C$ can be obtained by using the data in Figs. 10 and 11, Eqs. (6), (9), (11), (13), (14), and numerical calculation, as shown in Fig. 12. Besides, the curves of $\psi_{Rm} - \tilde{T}_H$ and $\psi_{Rm} - \tilde{T}_C$ under symmetry dissipation, namely, $\tilde{\sigma}_H = 0.5$, $\tilde{\sigma}_C = 0.5$, and $\beta = 0.5$, are plotted in Fig. 12 as well.

Besides, the behaviors of the maximum cooling power $\tilde{R}_{\max}$ and the corresponding optimal size ratio B_{Rm} varying with $\tilde{T}_H$ and $\tilde{T}_C$ are generated in the same way, as shown in Fig. 13. It can be found out from Fig. 13 that both $\tilde{R}_{\max}$ and B_{Rm} increase with the increase of $\tilde{T}_H$ and $\tilde{T}_C$ for given values of $\tilde{T}_C$ and $\tilde{T}_H$ at all three different dissipation conditions. This result can be explained as follows. As the temperature $\tilde{T}_H$ raises, the grade of the thermal energy from high-temperature reservoir improves. Therefore, a larger size Carnot refrigerator can be driven by a Carnot heat engine with the same size and higher cooling power can be obtained. Similarly, with the increase of $\tilde{T}_C$, the difficulty of absorbing heat from cooled space decreases. As a result, a Carnot heat engine with a given size can drive a larger size Carnot refrigerator and generate greater cooling power. In addition, Fig. 13 also shows that both $\tilde{R}_{\max}$ and B_{Rm} decrease with the increase of irreversibility (from upper bound to lower bound) for given values of $\tilde{T}_H$ and $\tilde{T}_C$. In other words, with the increase of irreversibility, a smaller Carnot refrigerator can be driven by a Carnot heat engine with given size and less cooling power can be obtained, which is an expected result due to the fact more thermal losses are generated by irreversibilities in all involved processes.

7. Discussions

7.1. The validity of the obtained bounds of ψ_{Rm}: Comparison with experimental and simulated data

In order to evaluate the validity of the proposed model and obtained bounds, the COPs of several typical thermally driven refrigerators reported in previous works by means of experimentation or simulation approaches are collected and listed in Table 1 together with the bounds of ψ_{Rm} obtained in the present paper. In addition, for the convenience of observation, a three-dimensional graph of ψ_{Rm} varying with $\tilde{T}_H$ and $\tilde{T}_C$ is further plotted by using the data in Fig. 12 and numerical calculation. It is presented in Fig. 14, where the data listed in Table 1 are marked by solid dots. It is worthy to point out that the values of $\tilde{T}_H$ and $\tilde{T}_C$ in Table 1 and Fig. 14 are obtained based on the temperature values from corresponding references and the definitions of $\tilde{T}_H$ and $\tilde{T}_C$, namely, $\tilde{T}_H = T_H/T_O$ and $\tilde{T}_C = T_C/T_O$. Table 1 and Fig. 14 clearly show that all the reported COPs are located in the region determined by the upper and lower bounds of ψ_{Rm}. In fact, not only those data in Table 1 and Fig. 14, but also many other reported COPs of thermally driven refrigerators [9,13,18,64] are consistent with the obtained bounds of ψ_{Rm} in the present paper, but they are not all displayed here for a clearer presentation of Fig. 14. From above results, it can be concluded that the model of LD THS refrigerator and the practical significance of the associated results are well validated.

Furthermore, it can be found out from Table 1 that most of the reported COPs are located between the lower bound of ψ_{Rm} and the ψ_{Rm} under symmetry dissipation, which can be explained as follows. On the one hand, thermally driven refrigerators are mainly driven by LG heat, namely, the temperature of the high-temperature is usually not so high. Therefore, the heat-transfer processes of the system are dominated by Newton's law. According to Refs. [38], the ψ_{Rm} obtained under symmetry dissipation in the LD model corresponds to the results obtained by adopting Newton heat-transfer law in endoreversible models. On the other hand, the external heat leakage losses, which exist in practical systems of thermally driven refrigerator, are not taken into consideration in the present paper. As a result, most of the reported COPs are close to and lower than the ψ_{Rm} obtained under symmetry dissipation, which indeed is a reasonable result.

It should be pointed out that in Table 1 and Fig. 14 some values of $\tilde{T}_H$ and $\tilde{T}_C$ are not obtained based on the temperatures of high-temperature reservoir T_H, environment T_O, and cooled space T_C due to the lack of these data. Instead, the temperatures of generator/desorber/hot water, condenser/absorber/adsorber/cooling water, and evaporator/chilled water have been adopted, respectively, to approximately calculate the values of $\tilde{T}_H$ and $\tilde{T}_C$, which possibly leads to the some deviations. Specifically, the obtained values of $\tilde{T}_H$ and $\tilde{T}_C$ will be slightly lower than the actual values. However, it can be seen from Fig. 14 that even if solid black dots move toward the direction of higher values of $\tilde{T}_H$ and $\tilde{T}_C$ slightly, most of them are still inside the region determined by upper and lower bounds of ψ_{Rm}. Consequently, the proposed model and the practical significance of the associated results are still valid.

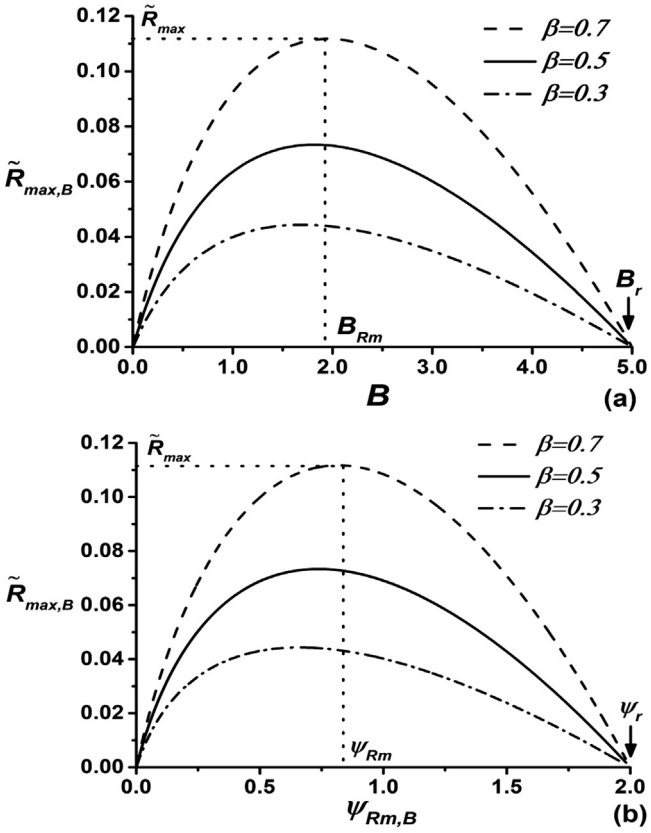

Fig. 10. The variations of $\tilde{R}_{\max,B}$ with (a) size ratio B and (b) the corresponding COP $\psi_{Rm,B}$ for different values of β. In all cases $\tilde{\sigma}_H = \tilde{\sigma}_C = 0.3$, $\tilde{T}_H = 2$ and $\tilde{T}_C = 0.8$.

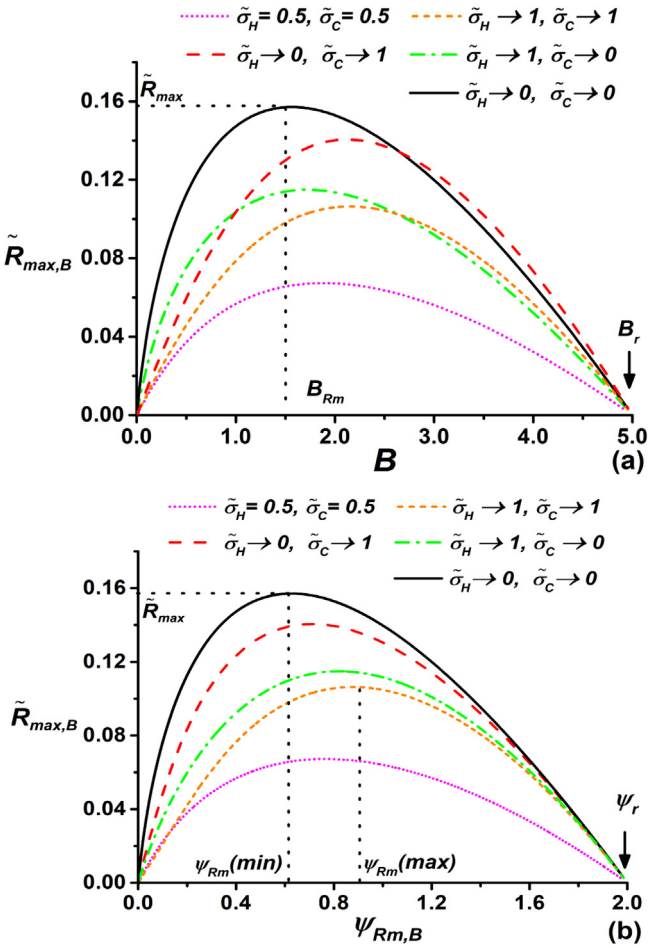

Fig. 11. The variations of $\tilde{R}_{max,B}$ with (a) size raito B and (b) the corresponding COP $\psi_{Rm,B}$ for different values of $\tilde{\sigma}_H$ and $\tilde{\sigma}_C$. In all cases $\beta = 0.5$, $\tilde{T}_H = 2$ and $\tilde{T}_C = 0.8$.

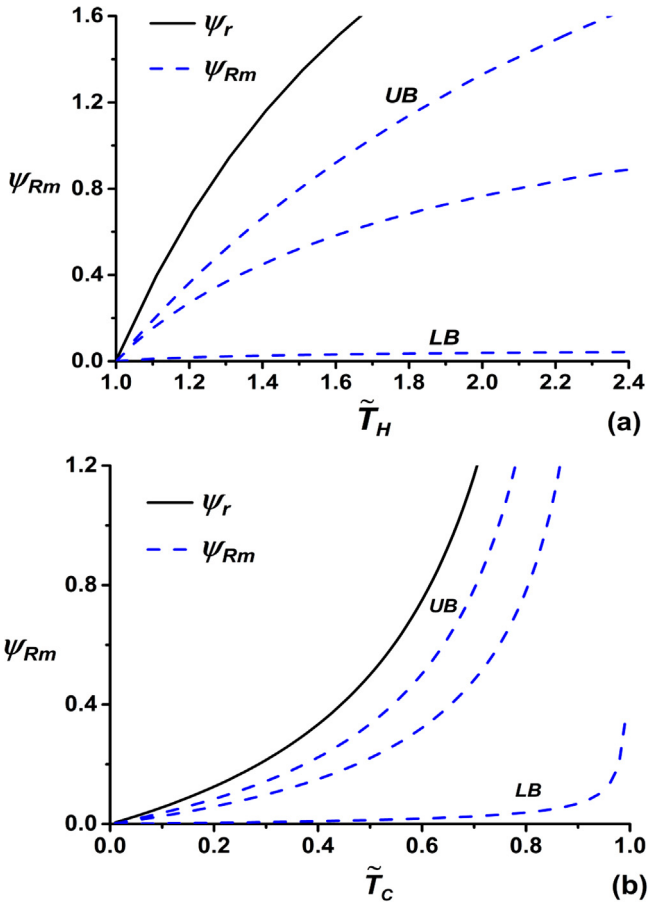

Fig. 12. The curves of ψ_{Rm} varying with (a) $\tilde{T}_H$ and (b) $\tilde{T}_C$ under various conditions: $\tilde{\sigma}_H \to 1$, $\tilde{\sigma}_C \to 1$, and $\beta \to 1$ for the upper bound (UB): $\psi_{Rm}(max)$ (see Fig. 11); $\tilde{\sigma}_H \to 0$, $\tilde{\sigma}_C \to 0$, and $\beta \to 0$ for the lower bound (LB): $\psi_{Rm}(min)$ (see Fig. 11); $\tilde{\sigma}_H = 0.5$, $\tilde{\sigma}_C = 0.5$, and $\beta = 0.5$ for the one between upper and lower bounds. (a) $\tilde{T}_C = 0.8$, (b) $\tilde{T}_H = 2$.

7.2. The limit case of $\tilde{T}_H \to \infty$: Traditional compression refrigerator

On the basis of Ref. [65], when the temperature of the high-temperature heat reservoir increases to infinity, it turns into a work source. Consequently, the proposed model of LD THS refrigerator shown in Fig. 2 becomes a conventional compression refrigerator working between cooled space and environment driven by electricity. In this case, $Q_H = W$, $Q_{OH} = 0$, $t_H = 0$, $t_{OH} = 0$, $\sigma_H = 0$, and $\sigma_{OH} = 0$. Besides, according to the definition of B and B_r, one can easily obtain $B = B_r \to \infty$ when $T_H \to \infty$, namely, the LD Carnot heat engine adopted in the LD THS refrigerator would not be exist. Furthermore, at this situation, Eqs. (1), (8), and (9) can be, respectively, simplified as

$$\psi_r = \frac{T_C}{T_O - T_C} \tag{15}$$

$$R = \frac{T_C \Delta S_{re}\left(1 - \frac{\sigma_C}{t_C}\right)}{t_{OC} + t_C} \tag{16}$$

and

$$\psi = \frac{T_C\left(1 - \frac{\sigma_C}{t_C}\right)}{T_O(1 + \frac{\sigma_{OC}}{t_{OC}}) - T_C(1 - \frac{\sigma_C}{t_C})} \tag{17}$$

Eqs. (15)–(17) are just the COP of the reversible refrigerator, the cooling power and COP of the LD Carnot refrigerator [39,44,45,48,66], respectively.

8. Conclusions and prospects

In the present paper, a more universal thermodynamic model of THS refrigerator without invoking any specific heat-transfer law has been constructed. It may be used to describe a variety of thermally driven refrigerators, e.g., absorption refrigerator, adsorption refrigerator, and ejector refrigerator. The following important findings are obtained:

1. A general description of the overall system of LD THS refrigerator with regard to temporal and dissipation symmetry was proposed, which extended the application scope of LD thermodynamic model [38] in theory and could be considered as another important step of the development of LD model. With the hel of the LD THS system were derived.
2. A key parameter $B = \Delta S_{re}/\Delta S_{he}$ accounting for the size ratio of Carnot refrigerator to Carnot heat engine has been defined by considering the practical implication of reversible entropy change inside the model. The parameter B plays an important role in connecting the two subsystems and it is of practical and theoretical significance. Based on the definition of B, the optimal relation between the COP and cooling power was obtained, according to which the optimal operation region and optimal construction of the LD THS system were further determined for the first time.
3. The influences of dissipation and temporal symmetries on the performance of the system were evaluated. In the light of the obtained performance characteristics, the most important achievement of the

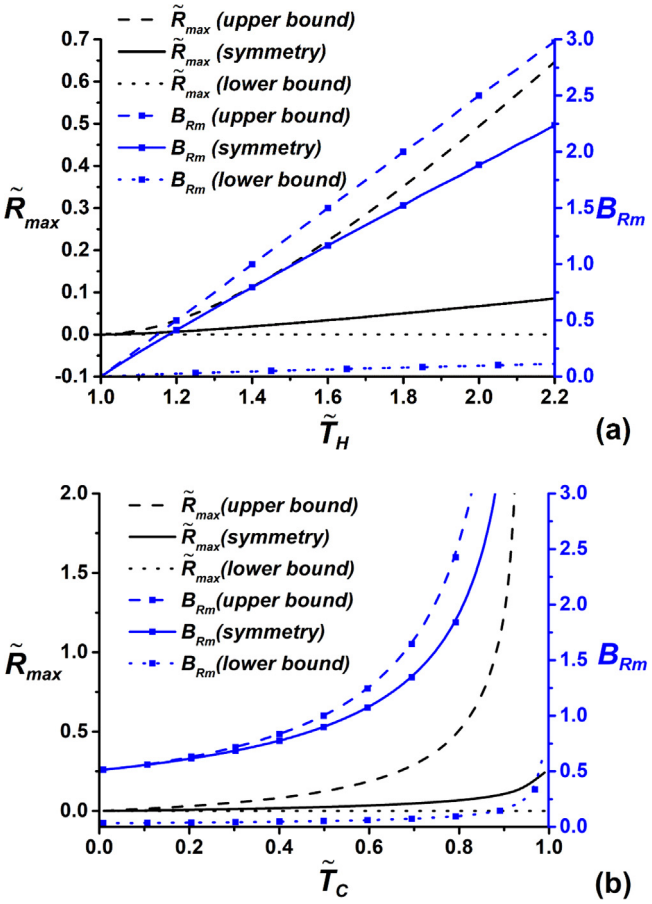

Fig. 13. The curves of $\tilde{R}_{\max}$ and B_{Rm} varying with (a) $\tilde{T}_H$ and (b) $\tilde{T}_C$ under various conditions: $\tilde{\sigma}_H \to 1$, $\tilde{\sigma}_C \to 1$, and $\beta \to 1$ for the upper bound; $\tilde{\sigma}_H \to 0$, $\tilde{\sigma}_C \to 0$, and $\beta \to 0$ for the lower bound; $\tilde{\sigma}_H = 0.5$, $\tilde{\sigma}_C = 0.5$, and $\beta = 0.5$ for the one between upper and lower bounds. (a) $\tilde{T}_C = 0.8$, (b) $\tilde{T}_H = 2$.

present paper, namely, the upper and lower bounds of the COP at maximum cooling power of the LD THS system, was obtained at two extreme dissipation asymmetry situations.

4. The experimental and simulated data from previous literatures were collected to verify the validity of the proposed LD THS model and the practical significance of the obtained upper and lower bounds. Besides, a limit case was given to emphasize the generality of the model.

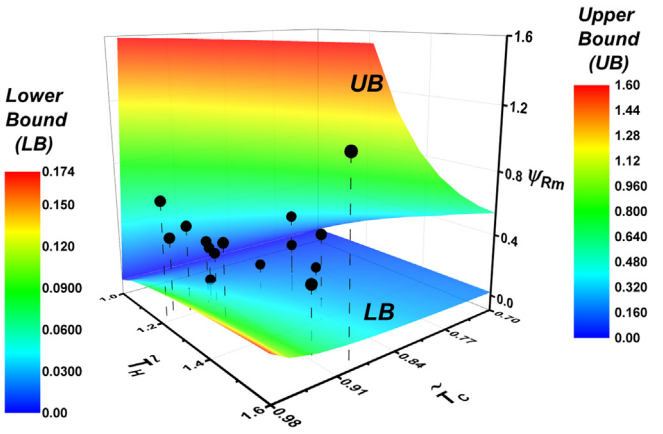

Fig. 14. Three-dimensional graph of ψ_{Rm} varying with $\tilde{T}_H$ and $\tilde{T}_C$ and the reported COPs collected in Table 1.

In conclusion, not only the application scope of LD thermodynamic model [38] has been successfully extended, but also more consistent results with reality for the thermally driven refrigerators have been obtained.

More importantly, the present paper provides a novel approach to investigate the performance of THS refrigerator, which can be further applied to reveal the performances of other thermodynamic devices operated between more than two energy reservoirs. In addition, various heat-transfer processes with finite values of heat capacity, e.g., isobaric and isochoric processes, can be introduced to make these LD model closer to reality. Different objective functions can be defined to evaluate the performance characteristics of those systems. Finally, the proposed LD thermodynamic model can be used to construct the hybrid systems with other specific systems such as solar collector, fuel cell, and so on, based on which the optimal modeling, coupling, and operation of the hybrid systems can be discussed. It is reasonable to believe that the achievements of the present paper enrich the theoretical thermodynamic model of thermally driven refrigerators and may provide some useful guidelines for the design and operation of realistic thermally driven refrigerators.

Declaration of Competing Interest

The authors declare that they have no known competing financial interests or personal relationships that could have appeared to influence the work reported in this paper.

Table 1
Reported COPs and the corresponding bounds of ψ_{Rm} obtained from the LD THS refrigerator model under specified temperatures.

Type of refrigerator	Reference	$\tilde{T}_H$	$\tilde{T}_C$	ψ_r	Reported COP	Bounds of ψ_{Rm} from the present paper			Inside the region
						Upper	Symmetry	Lower	(Y/N)
Absorption	[36]	1.30	0.934	3.24	0.433	1.83	1.11	0.0538	Y
Absorption	[53]	1.24	0.830	0.945	0.230	0.523	0.374	0.0226	Y
Absorption	[53]	1.24	0.830	0.945	0.427	0.523	0.374	0.0226	Y
Absorption	[54]	1.18	0.970	4.93	0.650	2.67	1.55	0.0698	Y
Absorption	[55]	1.40	0.850	1.62	0.450	0.944	0.612	0.0334	Y
Adsorption	[56]	1.18	0.943	2.52	0.460	1.36	0.881	0.0447	Y
Adsorption	[57]	1.18	0.853	0.885	0.0750	0.480	0.350	0.0215	Y
Adsorption	[57]	1.28	0.811	0.939	0.0770	0.527	0.373	0.0224	Y
Adsorption	[58]	1.20	0.967	4.88	0.430	2.66	1.55	0.0701	Y
Adsorption	[59]	1.58	0.888	2.91	1.07	1.78	1.03	0.0506	Y
Ejector	[60]	1.17	0.918	1.63	0.320	0.876	0.601	0.0330	Y
Ejector	[61]	1.16	0.912	1.43	0.0400	0.769	0.536	0.0301	Y
Ejector	[61]	1.16	0.912	1.43	0.260	0.769	0.536	0.0301	Y
Ejector	[62]	1.51	0.904	3.18	0.320	1.91	1.10	0.0537	Y
Ejector	[63]	1.17	0.908	1.43	0.225	0.774	0.537	0.0302	Y

Acknowledgements

This work has been supported by the National Natural Science Foundation of China (No. 11405032) and Junta de Castilla y León of Spain under project SA017P17. J.G.A. acknowledges University of Salamanca contract 2017/X005/1. In addition, Juncheng Guo thanks Rocio Yanes Diaz, Felipe Garcia-Sanchez, and all members of the thermodynamics research group at the University of Salamanca for the help they provided during his stay.

References

[1] Chu S, Majumdar A. Opportunities and challenges for a sustainable energy future. Nature 2012;488:294–303.
[2] Rahbar K, Mahmoud S, Al-Dadah RK, Moazami N, Mirhadizadeh SA. Review of organic Rankine cycle for small-scale applications. Energy Convers Manage 2017;134:135–55.
[3] Lee SW, Yang Y, Lee HW, Ghasemi H, Kraemer D, Chen G, et al. An electrochemical system for efficiently harvesting low-grade heat energy. Nat Commun 2014;5:3942.
[4] Guo J, Wang Y, Gonzalez-Ayala J, Roco JMM, Medina A, Calvo-Hernández A. Continuous power output criteria and optimum operation strategies of an upgraded thermally regenerative electrochemical cycles system. Energy Convers Manage 2019;180:654–64.
[5] Elsheikh MH, Shnawah DA, Sabri MFM, Said SBM, Hassan MH, Bashir MBA, et al. A review on thermoelectric renewable energy: principle parameters that affect their performance. Renew Sustain Energy Rev 2014;30:337–55.
[6] Wu W, Wang B, Shi W, Li X. Absorption heating technologies: a review and perspective. Appl Energy 2014;130:51–71.
[7] Wu X, Xu S, Jiang M. Development of bubble absorption refrigeration technology: a review. Renew Sustain Energy Rev 2018;82:3468–82.
[8] Kumar GP, Saravanan R, Coronas A. Simulation studies on simultaneous power, cooling and purified water production using vapour absorption refrigeration system. Appl Therm Eng 2018;132:296–307.
[9] Goyal P, Baredar P, Mittal A, Siddiqui AR. Adsorption refrigeration technology – An overview of theory and its solar energy applications. Renew Sustain Energy Rev 2016;53:1389–410.
[10] Alahmer A, Wang X, Al-Rbaihat R, Alam KCA, Saha BB. Performance evaluation of a solar adsorption chiller under different climatic conditions. Appl Energy 2016;175:293–304.
[11] Wang Y, Li M, Ji X, Yu Q, Li G, Ma X. Experimental study of the effect of enhanced mass transfer on the performance improvement of a solar-driven adsorption refrigeration system. Appl Energy 2018;224:417–25.
[12] Chen W, Shi C, Zhang S, Chen H, Chong D, Yan J. Theoretical analysis of ejector refrigeration system performance under overall modes. Appl Energy 2017;185:2074–84.
[13] Besagni G, Mereu R, Inzoli F. Ejector refrigeration: a comprehensive review. Renew Sustain Energy Rev 2016;53:373–407.
[14] Rashidi MM, Aghagoli A, Raoofi R. Thermodynamic analysis of the ejector refrigeration cycle using the artificial neural network. Energy 2017;129:201–15.
[15] Sur A, Das RK. Review on solar adsorption refrigeration cycle. Int J Mech Eng Technol (IJMET) 2010;1:190–226.
[16] Ahmadi MH, Ahmadi MA. Multi objective optimization of performance of three-heat-source irreversible refrigerators based algorithm NSGAII. Renew Sustain Energy Rev 2016;60:784–94.
[17] Wang RZ, Oliveira RG. Adsorption refrigeration-An efficient way to make good use of waste heat and solar energy. Prog Energy Combust Sci 2006;32:424–58.
[18] Chen J, Jarall S, Havtun H, Palm B. A review on versatile ejector applications in refrigeration systems. Renew Sustain Energy Rev 2015;49:67–90.
[19] Choudhury B, Saha BB, Chatterjee PK, Sarkar JP. An overview of developments in adsorption refrigeration systems towards a sustainable way of cooling. Appl Energy 2013;104:554–67.
[20] Huang FF. Engineering thermodynamics. New York: Macmillan; 1976.
[21] Wouagfack PAN, Tchinda R. Finite-time thermodynamics optimization of absorption refrigeration systems: a review. Renew Sustain Energy Rev 2013;21:524–36.
[22] Yan Z, Chen J. An optimal endoreversible three-heat-source refrigerator. J Appl Phys 1989;65:1–4.
[23] Wijeysundera NE. Performance of three-heat-reservoir absorption cycles with external and internal irreversibilities. Appl Therm Eng 1997;17:1151–61.
[24] Chen J. Optimal performance analysis of irreversible cycles used as heat pumps and refrigerators. J Phys D Appl Phys 1997;30:582–7.
[25] Göktun S. Optimal performance of an irreversible refrigerator with three heat source (IRWITHS). Energy 1997;22:27–31.
[26] Chen J, Schouton JA. Optimum performance characteristics of an irreversible absorption refrigeration system. Energy Convers Manage 1998;39:999–1007.
[27] Yan Z, Lin G. Ecological optimization criterion for an irreversible three-heat-source refrigerator. Appl Energy 2000;66:213–24.
[28] Nouadje BAM, Wouagfack PAN, Tchinda R. Influence of two internal irreversibilities on the new thermo-ecological criterion for three-heat-source refrigerators. Int J Refrig 2014;38:118–27.
[29] Kodal A, Sahin B, Ekmekci I, Yilmaz T. Thermoeconomic optimization for irreversible absorption refrigerators and heat pumps. Energy Convers Manage 2003;44:109–23.
[30] Zhang C, Li Y. Thermodynamic analysis on theoretical models of cycle combined heat exchange process: the reversible heat exchange process. Energy 2017;124:565–78.
[31] Bautista O, Mendez F, Cervantes JG. An endoreversible three heat source refrigerator with finite heat capacities. Energy Convers Manage 2003;44:1433–49.
[32] Bautista O, Mendez F. General performance of an irreversible three heat source refrigerator. Energy Convers Manage 2005;46:433–49.
[33] Chen L, Li Y, Sun F, Wu C. Optimal performance of an irreversible absorption refrigerator. Exergy Int J 2002;2:167–72.
[34] Chen L, Sun F, Chen W. Optimal performance coefficient and cooling load relationship of a three-heat-reservoir endoreversible refrigerator. Int J Power Energy Syst 1997;17:206–8.
[35] Fathi R, Guemimi C, Ouaskit S. An irreversible thermodynamic model for solar absorption refrigerator. Renew Energy 2004;29:1349–65.
[36] Wang F, Zhao J, Zhang H, Miao H, Zhao J, Wang J, et al. Efficiency evaluation of a coal-fired power plant integrated with chilled ammonia process using an absorption refrigerator. Appl Energy 2018;230:267–76.
[37] Yang P, Zhang H. Parametric analysis of an irreversible proton exchange membrane fuel cell/absorption refrigerator hybrid system. Energy 2015;85:458–67.
[38] Esposito M, Kawai R, Lindenberg K, Van den Broeck C. Efficiency at maximum power of low-dissipation Carnot engines. Phys Rev Lett 2010;105:150603.
[39] De Tomás C, Calvo-Hernández A, Roco JMM. Optimal low symmetric dissipation Carnot engines and refrigerators. Phys Rev E 2012;85:010104.
[40] Guo J, Wang J, Wang Y, Chen J. Universal efficiency bounds of weak-dissipative thermodynamic cycles at the maximum power output. Phys Rev E 2013;87:012133.
[41] Singh V, Johal RS. Low-dissipation Carnot-like heat engines at maximum efficient power. Phys Rev E 2018;98:062132.
[42] Long R, Liu W. Unified trade-off optimization for general heat devices with non-isothermal processes. Phys Rev E 2015;91:042127.
[43] Guo J, Cai L, Yang H, Lin B. Performance characteristics and parametric optimizations of a weak dissipative pumped thermal electricity storage system. Energy Convers Manage 2018;157:527–35.
[44] De Tomás C, Roco JMM, Calvo-Hernández A, Wang Y, Tu ZC. Low-dissipation heat devices: unified trade-off optimization and bounds. Phys Rev E 2013;87:012105.
[45] Wang Y, Li M, Tu ZC, Calvo-Hernández A, Roco JMM. Coefficient of performance at maximum figure of merit and its bounds for low-dissipation Carnot-like refrigerators. Phys Rev E 2012;86:011127.
[46] Gonzalez-Ayala J, Calvo-Hernández A, Roco JMM. Irreversible and endoreversible behaviors of the LD-model for heat devices: the role of the time constraints and symmetries on the performance at maximum χ figure of merit. J Stat Mech 2016;2016:073202.
[47] Ma YH, Xu D, Dong H, Sun C. Universal constraint for efficiency and power of a low-dissipation heat engine. Phys Rev E 2018;98:042112.
[48] Calvo-Hernández A, Medina A, Roco JMM. Time, entropy generation, and optimization in low-dissipation heat devices. New J Phys 2015;17:075011.
[49] Izumida Y, Okuda K. Efficiency at maximum power of minimally nonlinear irreversible heat engines. Europhys Lett 2012;97:10004.
[50] Izumida Y, Okuda K, Roco JMM, Calvo-Hernández A. Heat devices in nonlinear irreversible thermodynamics. Phys Rev E 2015;91:052140.
[51] Johal RS. Heat engines at optimal power: low-dissipation versus endoreversible model. Phys Rev E 2017;96:012151.
[52] Gonzalez-Ayala J, Santillán M, Santos MJ, Calvo-Hernández A, Roco JMM. Optimization and Stability of Heat Engines: the Role of Entropy Evolution. Entropy 2018;20:865.
[53] Said SAM, El-Shaarawi MAI, Siddiqui MU. Alternative designs for a 24-h operating solar-powered absorption refrigeration technology. Int J Refrig 2012;35:1967–77.
[54] Boudéhenn F, Demasles H, Wyttenbach J, Jobard X, Chèze D, Papillon P. Development of a 5 kW cooling capacity ammonia-water absorption chiller for solar cooling applications. Energy Proc 2012;30:35–43.
[55] Darwish NA, Al-Hashimi SH, Al-Mansoori AS. Performance analysis and evaluation of a commercial absorption-refrigeration water-ammonia (ARWA) system. Int J Refrig 2008;31:1214–23.
[56] Wang XL, Chua HT, Ng KC. Experimental investigation of silica gel-water adsorption chillers with and without a passive heat recovery scheme. Int J Refrig 2005;28:756–65.
[57] Oliveira RG, Silveira Jr V, Wang RZ. Experimental study of mass recovery adsorption cycles for ice making at low generation temperature. Appl Therm Eng 2006;26:303–11.
[58] Gong LX, Wang RZ, Xia ZZ, Chen CJ. Design and performance prediction of a new generation adsorption chiller using composite adsorbent. Energy Convers Manage 2011;52:2345–50.
[59] Amar NB, Sun LM, Meunier F. Numerical analysis of adsorptive temperature wave regenerative heat pump. Appl Therm Eng 1996;16:405–18.
[60] Nguyen VM, Riffat SB, Doherty PS. Development of a solar-powered passive ejector cooling system. Appl Therm Eng 2001;21:157–68.
[61] Shen S, Qu X, Zhang B, Riffat S, Gillott M. Study of a gas-liquid ejector and its application to a solar-powered bi-ejector refrigeration system. Appl Therm Eng 2005;25:2891–902.
[62] Kasperski J, Gil B. Performance estimation of ejector cycles using heavier hydrocarbon refrigerants. Appl Therm Eng 2014;71:197–203.
[63] Wang JH, Wu JH, Hu SS, Huang BJ. Performance of ejector cooling system with thermal pumping effect using R141b and R365mfc. Appl Therm Eng 2009;29:1904–12.
[64] Siddiqui MU, Said SAM. A review of solar powered absorption systems. Renew Sustain Energy Rev 2015;42:93–115.
[65] Andresen B, Salamon P, Berry RS. Thermodynamics in finite time: extremals for imperfect heat engines. J Chem Phys 1977;66:1571–7.
[66] Gonzalez-Ayala J, Medina A, Roco JMM, Calvo-Hernández A. Entropy generation and unified optimization of Carnot-like and low-dissipation refrigerators. Phys Rev E 2018;97:022139.